JOURNAL OF GEOPHYSICAL RESEARCH, VOL. 107, NO. A7, 1094, 10.1029/2001JA000152, 2002

Cross polar cap potentials measured with Super Dual Auroral Radar Network during quasi-steady solar wind and interplanetary magnetic field conditions

S. G. Shepherd,[1] R. A. Greenwald, and J. M. Ruohoniemi
Applied Physics Laboratory, Johns Hopkins University, Laurel, Maryland, USA

Received 30 May 2001; revised 12 October 2001; accepted 12 October 2001; published 4 July 2002.

[1] We have analyzed Super Dual Auroral Radar Network (SuperDARN) data between February 1998 and December 2000 to determine the statistical characteristics of the total variation in the high-latitude ionospheric electric potential, or cross polar cap potential, Φ_{PC}. Periods are chosen to satisfy the criteria that (1) the solar wind and interplanetary magnetic field (IMF) are quasi-stable for $\geq$40 min and (2) sufficient SuperDARN data exist to adequately determine Φ_{PC}. A total of 9464 individual 10-min periods satisfying the first criteria are analyzed. A subset of 2721 periods satisfy both criteria, of which 1638 are considered high-confidence periods. The resulting data set shows that for quasi-steady solar wind and IMF, Φ_{PC} (1) is nonlinear in the expression for the effective interplanetary electric field E_{KL}, (2) saturates at high values of E_{KL}, and (3) is highly variable for any given value of E_{KL}. These results indicate that simple formulations involving the upstream solar wind and IMF conditions are inadequate to describe the instantaneous Φ_{PC} and that the inclusion of internal and coupling processes between the magnetosphere and ionosphere may be necessary. *INDEX TERMS:* 2463 Ionosphere: Plasma convection; 2784 Magnetospheric Physics: Solar wind/magnetosphere interactions; 2736 Magnetospheric Physics: Magnetosphere/ionosphere interactions; 2411 Ionosphere: Electric fields (2712); *KEYWORDS:* convection electric field, cross polar cap potential and saturation, SuperDARN, interplanetary magnetic field

1. Introduction

[2] Large-scale electric fields resulting from a combination of viscous interactions and magnetic reconnection processes occurring at the magnetopause and in the magnetotail map along magnetic field lines with little attenuation into the high-latitude ionosphere. The total variation in the resulting ionospheric electric potential, referred to as the cross polar cap potential, or Φ_{PC}, is therefore an indicator of the amount of energy flowing into and through the magnetosphere-ionosphere (M-I) system. In addition to being an important parameter for describing the state of the magnetosphere, Φ_{PC} is useful for comparison with and validation of real-time and predictive space weather models.

[3] Several techniques have been used to measure Φ_{PC} and to study its correlation with solar wind drivers and other geophysical parameters. They include high-latitude, low-altitude spacecraft measurements of the convecting plasma velocity; Ogo 6 [*Heppner*, 1972], AE and S3 [*Reiff et al.*, 1981; *Reiff and Luhmann*, 1986; *Doyle and Burke*, 1983], DE 2 [*Weimer*, 1995, 1996, 2001], and Defense Meteorological Satellite Program (DMSP) [*Rich and Hairston*, 1994; *Boyle et al.*, 1997; *Burke et al.*, 1999]; assimilation and mapping of ground magnetometer and radar measurements such as the Assimilative Mapping of Ionospheric Electrodynamics (AMIE) technique [*Richmond and Kamide*, 1988]; linear regression relationships between solar wind parameters, ground-based magnetometers, and DMSP data such as the Institute of Terrestrial Magnetism, Ionosphere and Radiowave Propagation (IZMIRAN) Electrodynamic Model (IZMEM) [*Papitashvili et al.*, 1994] or the Linear Modeling of Ionospheric Electrodynamics (LiMIE) [*Papitashvili et al.*, 1999]; fitting backscattered ionospheric line-of-sight (LOS) convection velocities from ground-based radars to functional forms of the electrostatic potential [*Ruohoniemi and Baker*, 1998]; and global magnetospheric modeling such as the Lyon-Fedder-Moybarry (LFM) global magnetohydrodynamic (MHD) code [*Fedder and Lyon*, 1987; *Lyons*, 1998; *Slinker et al.*, 2001].

[4] Each of these techniques has limitations on the degree and accuracy to which it can determine or predict Φ_{PC}. Satellite measurements are spatially and temporally limited to the spacecraft orbit path, magnetometer data are spatially limited and must be inverted using ionospheric conductivity models, differences exist between global MHD models and observations possibly due to the lack of some necessary ionospheric physics in these models, radar measurements can be spatially limited, and parameterization techniques provide only typical or average values. The consequence is that comprehensive and definitive determinations of the ionospheric electric potential Φ and the associated Φ_{PC} have yet to be made.

[1]Now at Thayer School of Engineering, Dartmouth College, Hanover, New Hampshire, USA.

0148-0227/02/2001JA000152$09.00

[5] The technique developed by *Ruohoniemi and Baker* [1998], however, has some benefits over other techniques. This method involves fitting an expansion of spherical harmonic functions to Doppler measurements of the drifting ionospheric plasma provided by the Super Dual Auroral Radar Network (SuperDARN) coherent backscatter radars [*Ruohoniemi and Baker*, 1998], heretofore referred to as the Johns Hopkins University (JHU)/Applied Physics Laboratory (APL) fitting technique, or simply APL FIT. While SuperDARN is not exempt from spatial and temporal limitations, and sparse data from a statistical model [e.g., *Ruohoniemi and Greenwald*, 1996] are used to prevent nonphysical solutions in areas lacking measurements, the coverage provided by these radars is often a significant portion of the high-latitude ionosphere. Indeed, *Shepherd and Ruohoniemi* [2000] show that at times the coverage is sufficient to effectively determine a global solution of Φ in the high-latitude ionosphere based on the radar measurements. During such periods, and even during periods with less stringent data coverage requirements than shown by *Shepherd and Ruohoniemi* [2000], Φ_{PC} is well-defined by the APL FIT technique.

[6] In this study we use APL FIT to determine Φ_{PC} for 9464 10-min-averaged periods between 1 February 1998 and 31 December 2000. Solar wind conditions are provided by the Advanced Composition Explorer (ACE) satellite, orbiting around the so-called $L1$ Lagrangian point, for comparisons of Φ_{PC} with the solar wind conditions driving the ionospheric convection. The periods were chosen to minimize uncertainty in determining the geoeffective solar wind and interplanetary magnetic field (IMF) conditions and to occur during times when APL FIT provided a suitable determination of Φ_{PC}. The results presented in this study comprise the most comprehensive comparison of SuperDARN-determined Φ_{PC} and solar wind conditions to date.

2. Procedure

[7] To properly study the relationship between the solar wind driver of ionospheric convection and Φ_{PC}, care must be taken in selecting periods when (1) the measured solar wind conditions are known with some degree of certainty to be geoeffective and (2) the ionospheric data provide sufficient coverage in suitable locations to adequately define Φ_{PC}. The details of the selection criteria, and the subsequent decimations of the data are described in sections 2.1 and 2.3.

2.1. Solar Wind Selection Criteria

[8] For this study we use level 2 solar wind and IMF data provided by the ACE science team. ACE was chosen because (1) the satellite is reasonably stationary near the so-called $L1$ Lagrangian point, thus providing relatively uninterrupted monitoring of the solar wind conditions, and (2) the epoch of the satellite best matches the period when SuperDARN provides the most coverage (see section 2.3). The time range of this study is bounded by the availability of the ACE and SuperDARN data. The earliest ACE solar wind data are from February of 1998, and at the time of the study, SuperDARN data were available through December 2000. This study, therefore, extends from February 1998 through December 2000.

[9] To investigate the relationship between the solar wind and ionospheric convection, we choose to average the data over periods of 10 min. It is possible that by doing so we are missing the effects of variability with shorter timescales, but we question whether variability on such a short timescale is geoeffective to the large-scale convection. Therefore the level 2 Magnetometer Instrument (MAG) (16 s) and Solar Wind Electron Proton Alpha Monitor (SWEPAM) (64 s) are averaged over all 10-min periods bounded by the study time range, and a stability criteria is applied to the averaged data to determine which periods to include in the study.

[10] The primary reason for requiring quasi-stability of the solar wind and IMF is to minimize the effect that uncertainties inherent in determining the time delay between observation at $L1$ and the subsequent time of geoeffective impact in the ionosphere have on comparing the true solar wind conditions and the resulting ionospheric response. The uncertainty in timing the ionospheric response to IMF changes in the solar wind can be >10 min [e.g., *Ridley et al.*, 1998; *Collier et al.*, 1998; *Ridley*, 2000]. By requiring the solar wind to be quasi-stable for several 10-min-averaged periods, the solar wind and IMF conditions (in the averaged sense) measured at $L1$, when time-delayed using a standard technique, are certain to be geoeffective for some, if not all, of the 10-min periods. While uncertainties remain in the predicted delay time between measurements at $L1$ and in the ionosphere, the predicted geoeffective conditions during quasi-stable periods are statistically more accurate. In the extreme example the solar wind and IMF are both constants, and while the time delay may still be uncertain, the geoeffective solar wind conditions are known with absolute certainty. For this study we selected periods which satisfied the quasi-steady criteria for four or more consecutive 10-min averages, or $\geq$40 min.

[11] The definition of quasi-stability we choose for this study is

$$|\Delta E_{KL}|/E_{KL} < 7\%. \tag{1}$$

E_{KL} is an expression used by *Kan and Lee* [1979] for the effective interplanetary electric field and corresponds to the fastest merging rate at the subsolar magnetopause [*Sonnerup*, 1974] given by

$$E_{KL} = V B_T \sin^2(\theta/2), \tag{2}$$

where V is taken as the antisunward component of the solar wind velocity, $B_T = \sqrt{B_Y^2 + B_Z^2}$, and θ is the IMF clock angle in the $(Y - Z)_{\rm GSM}$ plane, or $\theta = \cos^{-1}(B_Z/B_T)$. ΔE_{KL} is the difference between the minimum and maximum values of E_{KL} during the entire $\geq$40-min period. Several other studies have used E_{KL} to demonstrate a correlation between the solar wind and Φ_{PC} [*Reiff et al.*, 1981; *Doyle and Burke*, 1983; *Weimer*, 1995; *Burke et al.*, 1999].

[12] An example period selected for this study is shown in Figure 1. Solid lines in Figures 1a–1f represent the level 2 ACE H^+ density, antisunward solar wind velocity, IMF magnitude, and IMF B_X, B_Y, and B_Z components, respectively. The quantities θ, B_T, and E_{KL} from equation (2) are shown in Figures 1g–1i, respectively. The period which satisfies equation (1) is marked by vertical dotted lines at 1300 and 1350 UT on 19 April 2000 in Figure 1. Between

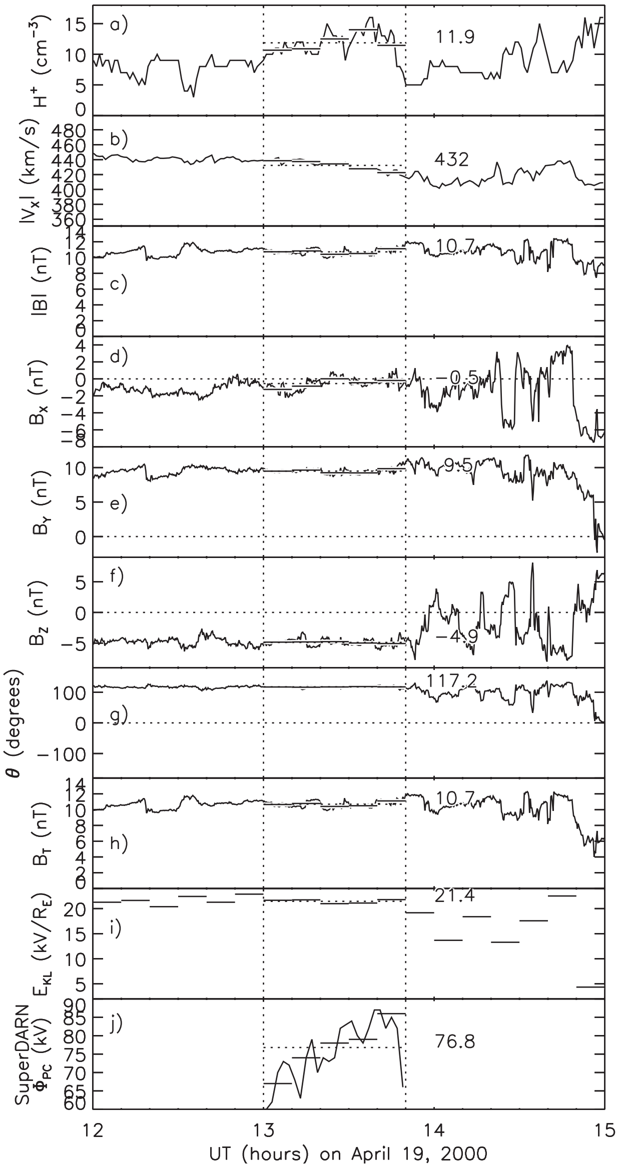

Figure 1. ACE solar wind and interplanetary magnetic field (IMF) data during a 50-min period of quasi-stable conditions beginning at 1300 UT on 19 April 2000, including (a) H^+ density, (b) antisunward solar wind velocity, (c) IMF magnitude, (d–f) IMF B_X, B_Y, and B_Z, (g) IMF clock angle θ, (h) B_T, (i) an expression for the interplanetary electric field E_{KL}, and (j) Φ_{PC} as determined by Applied Physics Laboratory (APL) fitting technique (FIT). The 10-min averages and averages for the 50-min period are shown in solid and dotted line segments, respectively.

these two times, 10-min averages of each quantity are indicated by horizontal thick line segments (E_{KL} is only calculated as 10-min averages, so it appears only as line segments), and a horizontal dotted line indicates the average value for the entire 50-min period, $\langle E_{KL} \rangle$ = 21.4 kV R_E^{-1}. Figure 1j shows Φ_{PC} determined using APL FIT (see section 2.3) at 2-min resolution as a solid line, at 10-min resolutions as horizontal line segments, and the average of Φ_{PC} over the five 10-min periods as a horizontal dotted line ($\langle \Phi_{PC} \rangle$ = 76.8 kV).

[13] Figure 2 shows the distribution of all the periods satisfying the quasi-stability criteria in equation (1) for three different percentages: 5, 7, and 10%. Figure 2a shows these distributions versus E_{KL} and, for comparison, versus the IMF B_Z component in Figure 2b. It can be seen that the general shape of the curves remains the same for the different percentages chosen, and thus the sampling is unbiased by the level of quasi-stability in the range 5–10%. We have selected 7% as a suitable value to use in equation (1) for this study. The choice of 7% increases the number of periods in the study from 5356 to 9464 over the 5% value, while maintaining a fairly restrictive stability requirement of the solar wind.

[14] The parameter E_{KL} dependzs on three solar wind quantities (IMF B_Z, IMF B_Y, and V), and uncertainty in its value depends on the uncertainties of these quantities. The ACE level 2 MAG data (IMF B_Z and B_Y) are stated to have errors of <.1 nT, and the ACE level 2 SWEPAM solar wind velocity data (V) are stated to have errors of <1%. Using these values, it is found that for E_{KL} > 2 kV R_E^{-1} the uncertainty in E_{KL} is < 4% and typically < 2%. For values of E_{KL} < 2 kV R_E^{-1}, which typically correspond to strongly northward IMF conditions with small (< ∼1 nT) IMF B_Y, the uncertainty in E_{KL} can be much larger. However, relatively few of the total periods in this study fall into this category as seen in Figure 2a.

2.2. Lag Time Determination

[15] In order to directly compare the solar wind measurements from ACE to the corresponding ionospheric radar measurements, and because the statistical model pattern

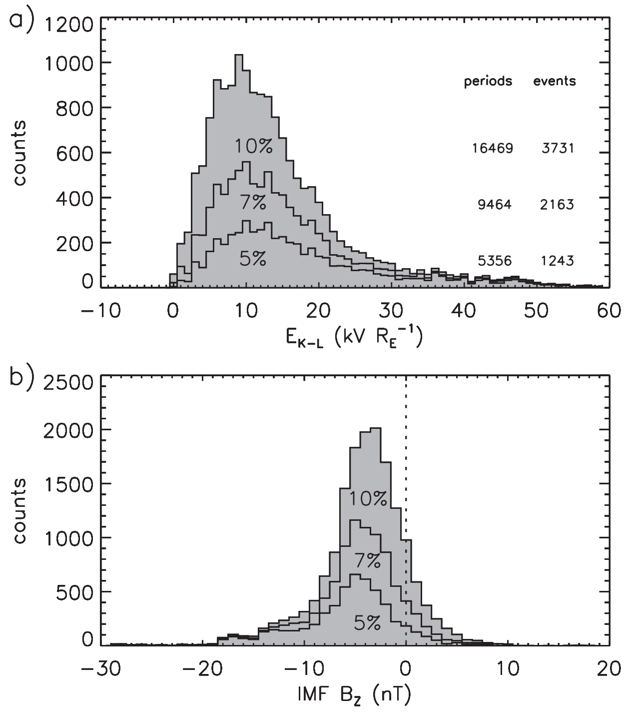

Figure 2. Distribution of study periods in (a) E_{KL} and (b) IMF B_Z using 5, 7, and 10% in equation (1). The middle value of 7% was selected for this study.

used in APL FIT is keyed to the IMF, we must determine the amount of time to delay the ACE measurements to allow for propagation to the ionosphere. This time delay, or lag time, between ACE and the ionosphere depends on the solar wind speed and density and can range from $\sim$30 min to longer than 90 min.

[16] The sensitivity to errors in the determination of the lag time is greatly reduced by selecting time periods with quasi-stable solar wind and IMF conditions. A nominal value for the lag time is found by applying a relatively standard technique, whereby the lag time is comprised of three parts: the solar wind advection time τ_{sw}, the magnetosheath transit time τ_{ms}, and the Alfvén transit time along magnetic field lines from the subsolar magnetopause to the ionosphere, τ_{alf}.

[17] The three components are given by

$$\tau_{sw} = (X_{sc} - X_{bs})/v_{sw}, \tag{3}$$

$$\tau_{ms} = \left(X_{bs} - X_{mp}\right)/v_{sw} \times 8, \tag{4}$$

$$\tau_{\mathrm{alf}} = 2 \text{ min}, \tag{5}$$

where X_{sc} is the position of ACE projected onto the Sun-Earth line, X_{bs} is the subsolar bow shock location following *Peredo et al.* [1995], X_{mp} is the subsolar magnetopause location following *Sibeck et al.* [1991, 1992], and v_{sw} is the antisunward solar wind speed (written as V in equation (1)). The 2-min value chosen for Alfvén transit time is the average of the 1–3 min thought to occur in practice [e.g., *Lester et al.*, 1993; *Khan and Cowley*, 1999]. The factor of 8 in equation (4) is due to the slowing of the plasma in the magnetosheath [*Spreiter and Stahara*, 1994].

2.3. Cross Polar Cap Potential Determination

[18] As mentioned in section 1, we use APL FIT to determine a global solution of Φ in the high-latitude ionosphere from which Φ_{PC} is easily found. *Ruohoniemi and Baker* [1998] give explicit details of this technique, and subsequent improvements are explained in the appendix of *Shepherd and Ruohoniemi* [2000]. Briefly, the LOS velocity measurements from each SuperDARN HF radar are mapped onto a grid of roughly equal area cells ($\sim$110 km $\times$ 110 km) in the region >50° latitude, using the geomagnetic coordinate system described by *Baker and Wing* [1989]. Additional data vectors from the statistical model of *Ruohoniemi and Greenwald* [1996] are sparsely added to the grid in order to prevent the solution from becoming nonphysical in regions where no data are available. The choice of the particular model data is determined by the magnitude and orientation of the IMF conditions at the magnetopause.

[19] An expression for Φ is obtained by fitting the LOS and model data to an expansion of spherical harmonic basis functions. The order of the expansion is chosen in such a manner as to represent the global character of the convection while retaining local features observed by the radars. For this study all fittings were performed to order 8.

[20] Figure 3 shows the solution of Φ obtained from APL FIT for the example period in Figure 1. Each 10-min period is shown on a grid of magnetic local time (MLT) and magnetic latitude $\geq$60° [*Baker and Wing*, 1989]. The locations of SuperDARN measurements are denoted by markers consisting of dots and vector tails. The tail points in the direction of the solved velocity at that location, and its length indicates the magnitude according to the scale in the upper right corner of Figure 3.

[21] Contours of Φ are spaced at 6-kV intervals. The potential extrema are indicated in each cell by a plus sign and negative sign for the dawn and dusk cells, respectively. Φ_{PC} is simply the difference between these two values and is shown in the lower left corner of each plot. In the lower right corner the $(Y - Z)_{\mathrm{GSM}}$ components of the IMF, measured at ACE and lagged according to equations (3), (4), and (5), are shown.

[22] The fitted solutions of Φ in Figures 3a–3e show a two-cell convection pattern with antisunward flow over the polar cap and sunward return flow along the dawn and dusk flanks that is typical of IMF $B_Z < 0$. Evidence of the relatively strong ($\sim$10 nT) IMF $B_Y > 0$ can be seen in the dayside ionosphere in the form of flow toward the dawn sector across 1200 MLT between 75° and 80° and the existence of a more crescent-shaped dawn cell and a more circular dusk cell [*Heppner*, 1972; *Crooker*, 1979; *Heelis*, 1984; *Reiff and Burch*, 1985; *Greenwald et al.*, 1990].

[23] During the example period shown in Figures 3a–3e, backscatter from SuperDARN HF radars was observed over a large region of the dayside between $\sim$0600 and 1800 MLT and, in some areas, from <65° to nearly 90° latitude. There is also a large region of the postmidnight sector from which backscatter was observed. During this period, Φ is much more structured than statistical models would prescribe for the given IMF [e.g., *Ruohoniemi and Greenwald*, 1996; *Weimer*, 2001]. While mesoscale structures evolve throughout the 50-min period, the main feature of these patterns is the steady increase in Φ_{PC}, from 67 to 86 kV, attributed to an expansion of the region containing large (>1 km s^{-1}) zonal velocities in the postnoon dayside sector and the increase in large sunward velocities in the dusk sector around 0400 MLT.

[24] Figure 1j shows a time series of Φ_{PC} during this period. The solid line represents Φ_{PC} as determined using APL FIT with the standard 2-min resolution SuperDARN data [*Greenwald et al.*, 1995]. The 10-min averaged Φ_{PC} values and the average for the entire 50-min period are shown as solid and dotted horizontal line segments, respectively.

[25] Despite the quasi-stable solar wind and IMF conditions, there is quite large variability in Φ_{PC}. The range of the 10-min-averaged Φ_{PC} is 67–86 kV, and the range of the 2-min Φ_{PC} is 60–87 kV.

[26] For this study a solution of Φ is determined using APL FIT for each 10-min period that satisfies equation (1). For each of these periods the number of data points (a data point is defined as a grid cell containing LOS data from a single SuperDARN radar) in each MLT sector is extracted and used to select a subset of periods for which the SuperDARN data provide sufficient coverage to adequately define Φ_{PC}. While complete coverage of the entire high-latitude ionosphere is ideal for a truly definitive determination of Φ_{PC}, this situation never occurs in practice. It is, however, possible to accurately determine Φ_{PC} with significantly less coverage. For instance, a "polar cap" determination of Φ_{PC} is possible by measuring only the flow in the polar cap region between the two potential extrema. Like-

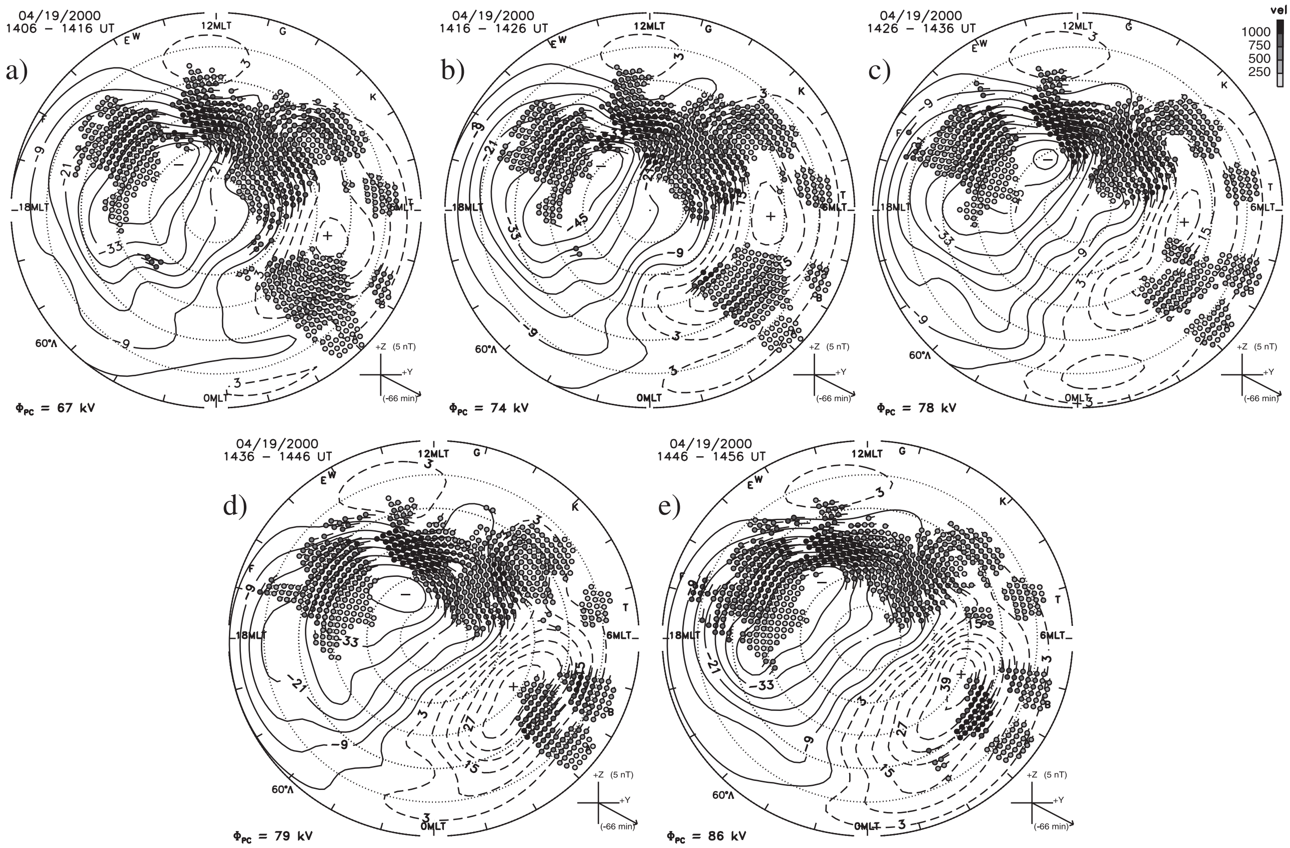

Figure 3. Solutions of the electrostatic potential Φ using APL FIT for the example period shown in Figure 1. The lag time of the IMF measured at ACE is calculated using equations (3), (4), and (5), and the fitting is performed to order 8. Arrows indicate the position of SuperDARN measurements and denote the direction of the fitted velocity determination at that location. The magnitude of each fitted velocity determination is indicated by the length of the arrow. Contours are spaced at 6-kV increments to represent the electrostatic potential Φ.

wise, an "auroral" determination of Φ_{PC} is also possible by measuring only the flow at latitudes below each of the potential extrema. Our usual approach is the "polar cap" solution, which, in practice, can be obtained with as few as two SuperDARN radars, provided the backscatter is sufficient in extent and the radars are making measurements in the proper MLT sector (usually the dayside near 1200 MLT and looking into the convection throat). Periods with much less than total coverage of the high-latitude ionosphere can therefore be suitable for determining Φ_{PC}.

[27] Several definitions of adequate coverage are possible, and after trying various formulations involving the number and location of data points we define suitable coverage as those times when >200 data points exist in the dayside (0600–1800 MLT) ionosphere or >400 data points exist anywhere in the high-latitude region. This criteria does not guarantee that SuperDARN measurements are made over the entire region spanning the potential extrema, but it is our experience that this is most often the case. More than 200 data points in the dayside region almost always ensures that the convection throat region is adequately sampled, and more than 400 data points overall includes periods when the nightside convection out of the throat is well-defined and periods when the polar cap is contracted and the former criteria is overly restrictive.

[28] One final selection criteria is imposed on the data set. Because there is some uncertainty in the propagation time of the solar wind observations at ACE, the first and last 10-min period of each quasi-stable period $\geq$40 min is dropped from the final data set to allow for $\pm$10 min uncertainty in the propagation time.

[29] To summarize the various restrictions imposed on the data sets and the corresponding decimations to the number of periods included in the study, we begin by selecting quasi-stable periods of the solar wind and IMF conditions. A total of 9464 10-min periods result from searching the ACE level 2 MAG and SWEPAM data for events that satisfy equation (1) for $\geq$40 min. Of these matches, 2721 10-min periods satisfy the condition that either >200 SuperDARN data points are present in the dayside sector or >400 total SuperDARN data points are present in the high-latitude region. Finally, the first and last 10-min periods for each event lasting $\geq$40 min are dropped, reducing the number of periods to 1638. This subset of 10-min periods represents those times when (1) the solar wind driving conditions at the magnetopause and (2) the convection in the dayside high-latitude ionosphere

are both well-known. These high-confidence periods form the basis of our statistical study of Φ_{PC} and the solar wind driver.

3. Results

[30] For comparison purposes, Φ_{PC} is calculated using APL FIT for all 9464 10-min periods satisfying the quasi-stability condition imposed on the solar wind and IMF in equation (1) in addition to the subset of 1638 high-confidence periods described in section 2.3. Figure 4 shows the resulting values of Φ_{PC} versus E_{KL} for both sets of 10-min periods. A histogram on the right of each plot shows the distribution of Φ_{PC} values. For each whole number of E_{KL} up to 40 kV R_E^{-1} a sliding, linear least squares fit was performed to the data within a 10 kV R_E^{-1} window centered on that value. The resulting fit and corresponding 2σ standard deviations are shown as dark line segments bounded by lighter line segments. For the data in the range E_{KL} > 40 kV R_E^{-1} a single fit was performed due to the sparsity of data at high values of E_{KL}. Four specific 10-min periods are shown by larger dots and marked by the numbers 0–3. The APL FIT solutions for these four periods are shown in later figures.

[31] Several noteworthy features of the data are illustrated by Figure 4. Of particular note is the similarity between the entire set of 9464 10-min periods (Figure 4a) and the subset of 1638 high-confidence periods (Figure 4b). Except for very large values of E_{KL} (>~60 kV R_E^{-1}), the data distributions have much the same character for both sets of periods. For E_{KL} < 40 kV R_E^{-1} the fitted line segments for both data sets have similar values, slopes, and standard deviations (above ~30 kV R_E^{-1}, low statistics begin to affect the slope determinations). Because the set of all 10-min periods is determined without regard to the degree of data coverage from the SuperDARN radars, it includes periods when the SuperDARN data are insufficient to fully define Φ_{PC}, and Φ_{PC} is consequently determined to a large degree by the statistical model. The similarity between the two data sets for E_{KL} <~40 kV R_E^{-1} therefore implies that Φ_{PC} of the statistical model patterns used in APL FIT are accurate in the statistical sense with those values calculated from the high-confidence periods, i.e., when the SuperDARN data adequately constrain the solution of Φ_{PC}. Of course, the inherent nature of statistical quantities ensures that the convection patterns derived by *Ruohoniemi and Greenwald* [1996] appear smoothed or averaged when compared to any particular solution of Φ; however, it seems that Φ_{PC} is well-defined statistically by these patterns for E_{KL} < ~40 kV R_E^{-1}.

[32] The trends for E_{KL} > 40 kV R_E^{-1} are somewhat different between the two data sets. In Figure 4a the best fit line segment to the data from the entire set of 10-min periods is roughly flat in this range, but Figure 4b shows a definite increase in the mean Φ_{PC} as E_{KL} increases. Part of the reason for this difference is due to the statistical models used in APL FIT. Values of E_{KL} larger than 40 kV R_E^{-1} correspond to IMF B_Z < 0 with a magnitude > ~12 nT. The largest IMF magnitude bin of *Ruohoniemi and Greenwald* [1996] is 6–12 nT, where the mean value of the IMF for the data used to construct these patterns was ~7 nT. Consequently, for some of the periods shown

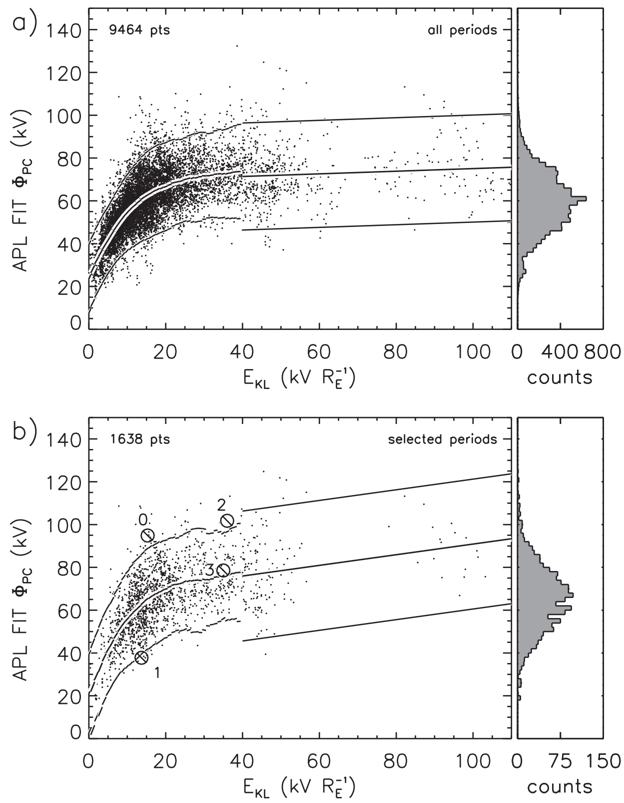

Figure 4. Φ_{PC} as a function of E_{KL} determined using APL FIT for (a) all 10-min periods satisfying equation (1) and (b) those periods where the SuperDARN data sufficiently determine Φ_{PC} (see section 2.3). Each 10-min period is represented by a dot. A sliding, linear least squares fit to data within a 10 kV R_E^{-1} window, and corresponding 2σ deviations, are shown for each unit of E_{KL} up to 40 kV R_E^{-1}. Because of the sparsity of data in the range E_{KL} > 40 kV R_E^{-1}, a single fit was performed on this data. Four larger dots indicate specific periods shown in later figures.

in Figure 4a, where E_{KL} > 40 kV R_E^{-1} and the data coverage is below our threshold, Φ_{PC} is determined to a large extent by the statistical models, which most likely underestimate Φ_{PC} for the largest values of E_{KL}. The full range of Φ_{PC} is therefore not represented in the determination of the mean for E_{KL} > 40 kV R_E^{-1} in Figure 4a. Hence the mean is lower than it is for the high-confidence periods in Figure 4b for which the statistical models have much less impact.

[33] Another obvious feature in Figure 4 is the significantly nonlinear relationship between Φ_{PC} and E_{KL}. The slope of each line segment fit to the data in Figure 4 steadily decreases as E_{KL} increases; that is, there is no evident range of E_{KL} where Φ_{PC} is truly linear. In contrast to these results are the linear relations of Φ_{PC} determined in other studies. *Burke et al.* [1999] use the same data from DE 2 and the same technique used by *Weimer* [1995, 1996] to show that Φ_{PC} is linear to a very good agreement with E_{KL} for values <30 kV R_E^{-1} (Figure 3a [*Burke et al.*, 1999]). However, it should also be noted that in the same study, and using a

limited range of S3-2 data, this linear relationship appears much less convincing, and much more scatter is evident in the data (Figure 3d [*Burke et al.*, 1999]).

[34] In another study that uses low-altitude, high-latitude spacecraft measurements of drifting ionospheric plasma to estimate Φ_{PC}, *Boyle et al.* [1997] determine an empirical relationship for Φ_{PC} given by

$$\Phi_{PC} = 10^{-4}v^2 + 11.7B\sin^3(\theta/2) \quad \text{kV}, \tag{6}$$

where v is the solar wind velocity in km s^{-1}, B is the magnitude of the IMF in nanoteslas, and $\theta = \cos^{-1}(B_Z/B)_{\mathrm{GSM}}$. Figure 5 shows the results of applying equation (6) to the solar wind conditions measured during all of the periods used in the study as well as sliding, linear least squares fits and 2σ deviations to these calculated values for direct comparison to the APL FIT results shown in Figure 4. While the relation in equation (6) is not strictly linear in E_{KL}, the data follow a linear trend to good agreement.

[35] Figures 4 and 5 illustrate the two differing views of the relationship between Φ_{PC} and the merging electric field. The APL FIT data suggest that Φ_{PC} is nonlinearly related to the merging electric field and saturates at large values of E_{KL}, while the *Boyle et al.* [1997] model suggests that Φ_{PC} continues to increase without limit. While the lower limit of Φ_{PC} is ~20 kV for both data sets, the APL FIT data show a deviation from linearity for values of E_{KL} even below ~20 kV R_E^{-1}. To better show the different behavior of the two data sets, Figure 6 shows the slopes of the line segments for E_{KL} < 50 kV R_E^{-1} from Figures 4 and 5. Note that above ~30 kV R_E^{-1} the statistics are low, causing the fittings to be somewhat erratic above these values. A second set of axes are added to Figure 6 to show the value of an effective IMF B_Z if the IMF is assumed to be purely southward and a nominal value of 450 km s^{-1} is assumed for the solar wind speed. The trends in the data, shown by dashed lines, illustrate that Φ_{PC} using APL FIT saturates, while the *Boyle et al.* [1997] model does not.

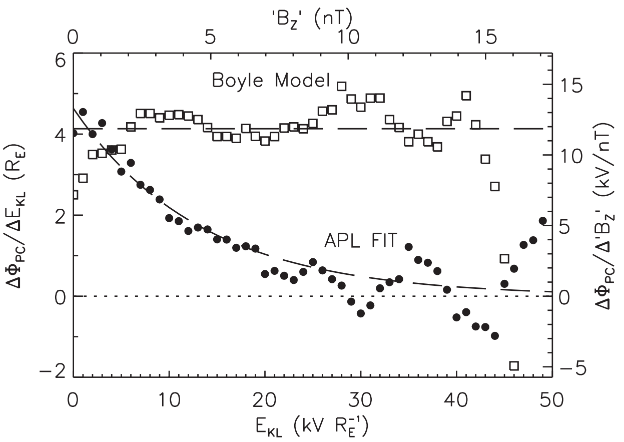

Figure 6. Slopes of the linear least squares fits to 10 kV R_E^{-1} wide ranges of E_{KL}, shown as line segments in Figures 4b (dots) and 5b (squares). Saturation of Φ_{PC} for large values of E_{KL} is suggested by the APL FIT data, in contrast to a linear trend evident in the *Boyle et al.* [1997] model data. Statistics are low for E_{KL} >~30 kV R_E^{-1}.

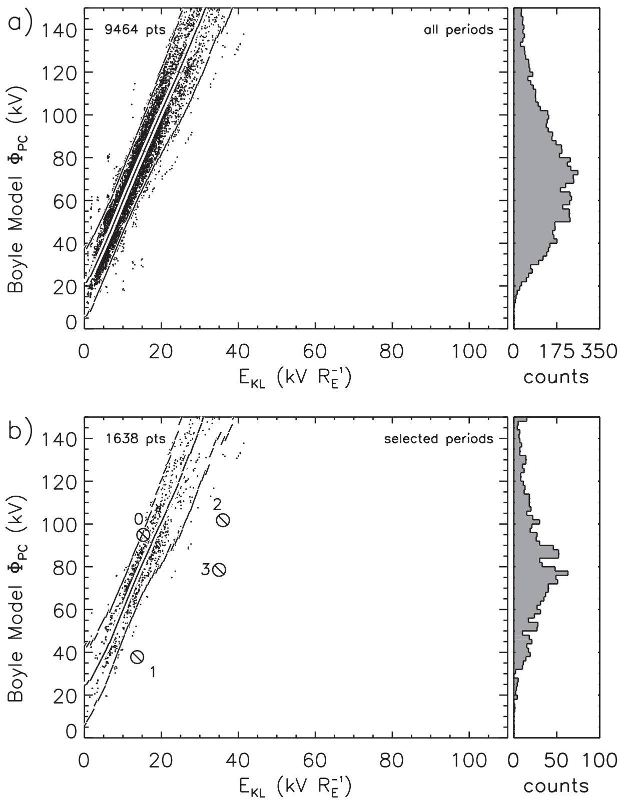

Figure 5. Φ_{PC} computed from the solar wind observations of this study using the model of *Boyle et al.* [1997] for the periods shown in Figure 4. A sliding, linear least squares fit to the data and 2σ deviations are computed and shown in the same format as Figure 4.

[36] It has long been theorized that Φ_{PC} saturates during extremely strong IMF conditions [*Hill et al.*, 1976]. Supporting this idea, some earlier studies using low-altitude spacecraft found that Φ_{PC} rarely exceeded 160 kV [*Reiff et al.*, 1981; *Reiff and Luhmann*, 1986]. There are reports of Φ_{PC} reaching values of 230 kV during storm periods [e.g., *Sojka et al.*, 1994], and *Boyle et al.* [1997], using a larger data set of low-altitude spacecraft that included DMSP, found that there is no evidence of saturation of Φ_{PC}. It should, however, be noted that because the more desirable dawn-dusk DMSP passes normally used to determine Φ_{PC} were limited in number for large IMF, *Boyle et al.* [1997] used a fitting technique to estimate Φ_{PC} for DMSP passes in all MLT sectors. It should also be noted that in their study the observed total potential variation was rarely observed to exceed 150 kV. For the largest values of E_{KL} (>100 kV R_E^{-1}) in our study the model given by equation (6) predicts values of Φ_{PC} that exceed 450 kV, which to our knowledge, have not been observed. More recently, *Siscoe et al.* [2002] show evidence during storm periods that Φ_{PC} does indeed saturate for large values of the solar wind electric field.

[37] The question of whether the ionosphere can support such large values of Φ_{PC} or whether saturation occurs is an important aspect of M-I coupling. How the ionospheric convection electric field and the magnetospheric and ionospheric currents systems interact in a self-consistent manner is still an unresolved issue. The evidence we show in

favor of saturation is that Φ_{PC} is nonlinear throughout the range of E_{KL} shown here and that Φ_{PC} has an upper limit of $\sim$150 kV. Figure 6 shows the trend of $\Delta\Phi_{PC}/\Delta E_{KL}$ steadily decreasing with increasing E_{KL}. In addition, for no period in the entire study does Φ_{PC} exceed 130 kV, even for very large values of E_{KL}. In fact, it is rare for Φ_{PC} to exceed $\sim$140 kV using the APL FIT technique as described by *Ruohoniemi and Baker* [1998] and *Shepherd and Ruohoniemi* [2000], even at 2-min resolution [e.g., *Shepherd et al.*, 2000].

[38] It should be noted, however, that while the data from this study suggest that saturation of Φ_{PC} occurs, difficulties arise in using the APL FIT technique for large values of IMF $B_Z < 0$ and E_{KL}. The problem occurs when the coupling between the solar wind and magnetosphere is exceptionally favorable for extended periods of time, and the rapidly reconnecting magnetic flux at the dayside magnetopause causes the lower latitude boundary of convection to expand to magnetic latitudes equatorward of $\sim$55°. The SuperDARN radars in the Northern Hemisphere are located between 56° and 65° magnetic latitude. Because of the propagation conditions necessary to achieve perpendicularity to the magnetic field at ionospheric altitudes and detect backscatter, the effective lowest magnetic latitude for observing backscatter tends to range from 58° to 63°, depending on the radar. That being said, because the convection region is constrained to relatively higher magnetic latitudes on the dayside [e.g., *Heppner and Maynard*, 1987], significant coverage of the dayside region and therefore determination of Φ_{PC} can be achieved even when the convection region is expanded to below 50° on the nightside.

[39] In order to determine better whether the statistical results of Figure 4 actually confirm that Φ_{PC} saturates at high values of E_{KL}, we look at several individual periods from the study in more detail. Figures 7a, 7b, 8a, and 8b, show the solutions of APL FIT for the four periods labeled 0–3, respectively, in Figure 4b. These periods are chosen to illustrate relatively high and low values of Φ_{PC} for two values of E_{KL}, $\sim$15 kV R_E^{-1} and $\sim$35 kV R_E^{-1}.

[40] The APL FIT solutions for the periods 0514–0524 UT on 19 March 2000 and 1748–1758 UT on 30 March 2000 are shown in Figure 7. For these periods, E_{KL} = 15.3 kV R_E^{-1} and 13.7 kV R_E^{-1}, respectively. Despite roughly equal values of E_{KL}, lower latitude limits of convection ($\sim$65°), and the amount of SuperDARN data coverage, the resulting values of Φ_{PC} (95 and 37 kV) are dramatically different. For both periods the SuperDARN data coverage is sufficiently extended and suitably located to adequately define the solution of Φ_{PC}. The difference between these two periods is that the observed convection on 19 March 2000 is dominated by a large region of flow >1 km s^{-1} in the dayside convection throat region, while on 30 March 2000 the convection is observed over most of the high-latitude dayside to be exclusively <1 km s^{-1}. The character of the convection and hence Φ_{PC} is dramatically different for these two periods.

[41] Figure 8 shows the APL FIT solutions for the periods 1622–1632 UT on 26 September 1999 and 2252–2302 UT on 22 January 2000. For these periods, E_{KL} = 36.0 kV R_E^{-1} and 35.0 kV R_E^{-1}, while Φ_{PC} = 98 and 78 kV, respectively. Despite the lower latitude convection boundary extending below 60°, in both cases there is good coverage from the SuperDARN radars. The convection on 26 September 1999 shows two regions of flow >1 km s^{-1} in the prenoon dayside and dusk sectors, as would be expected for higher values of E_{KL} and more effective penetration of the solar wind electric field. On 22 January 2000 the convection is observed from 1100–0100 UT to be exclusively <1 km s^{-1}. For both of these cases the true Φ_{PC} is most likely somewhat higher than the computed values given the expanded nature of the convection region; however, the 22 January 2000 period clearly indicates that Φ_{PC} is much less than the $\sim$188-kV potential predicted by the *Boyle et al.* [1997] model given by equation (6).

[42] These four periods reinforce the nonlinear trend of Φ_{PC} shown in Figure 4b and the low values of Φ_{PC} like that in Figure 8b, and together with a maximum value of $\sim$125 kV for this study these periods strongly suggest that Φ_{PC} does indeed saturate at high values of E_{KL}. Because of the difficulty previously mentioned in achieving backscatter during times when the convection region is expanded to midlatitudes, the saturation value is most likely above the 125-kV maximum observed. It should also be emphasized that these results are for 10-min-averaged periods during which the solar wind and IMF conditions are quasi-stable for $\geq$40 min. A different conclusion is possible for periods of nonsteady solar wind and IMF conditions; however, since it has recently been demonstrated that ionospheric convection responds rapidly (< $\sim$2 min) to changes in the IMF [*Ruohoniemi et al.*, 2002, and references therein], these results are likely to also apply during more dynamic conditions.

[43] Another important aspect shown by the data in Figure 4 and emphasized in Figures 7 and 8 is the amount of variability in Φ_{PC} for all values of E_{KL}. Where the statistics are greatest ($\sim 5 \geq E_{KL} \geq \sim 20$), the standard deviations of the line segment fittings are 9–12 kV. Similar values are found for the other ranges of E_{KL}, but the statistics are lower. These rather large variations are surprising given the stability of the solar wind and IMF during these periods. The solid line in Figure 1j shows that Φ_{PC} determined using APL FIT with the standard 2-min resolution SuperDARN data is even more variable than the 10-min-averaged data.

[44] It is possible that the solar wind and IMF change enough during the transit from ACE through the solar wind and the magnetosheath to account for the observed variability in Φ_{PC}; however, several studies suggest that the solar wind remains relatively unchanged over this distance [e.g., *Prikryl et al.*, 1998]. *Maynard et al.* [2001] claim that even small-scale structure in E_{KL} measured 200 R_E upstream in the solar wind remains coherent to a remarkable degree into the dayside ionospheric cusp.

[45] Since Φ_{PC} is a global parameter and the ionosphere requires a finite amount of time to reconfigure to changes at the magnetopause [*Ruohoniemi et al.*, 2002], small-scale fluctuations in E_{KL} most likely have little affect on Φ_{PC}. It is more likely that some internal processes such as variable ionospheric conductivity due to particle precipitation or variable reconnection rates in the magnetotail are responsible for the large variability in Φ_{PC}. Theories have long suggested that the ionosphere is capable of regulating magnetospheric convection [*Coroniti and Kennel*, 1973].

It is apparent that a more complicated expression that includes the contribution of magnetic field line merging in the magnetotail is needed to fully describe the dynamics of Φ_{PC} and its relationship to other geophysical parameters. It is undoubtedly the case that reconnection in the magnetotail, possibly during substorms, will contribute to Φ_{PC}, and it is possible that some models of ionospheric flow [e.g., *Siscoe and Huang*, 1985] would account for the observed variability in Φ_{PC} during quasi-stable solar wind conditions. *Siscoe et al.* [2002] attempt to provide a more comprehensive description of the behavior of Φ_{PC} by proposing a model based on the work of *Hill et al.* [1976]. In their study an expression for Φ_{PC} is given that includes a contribution

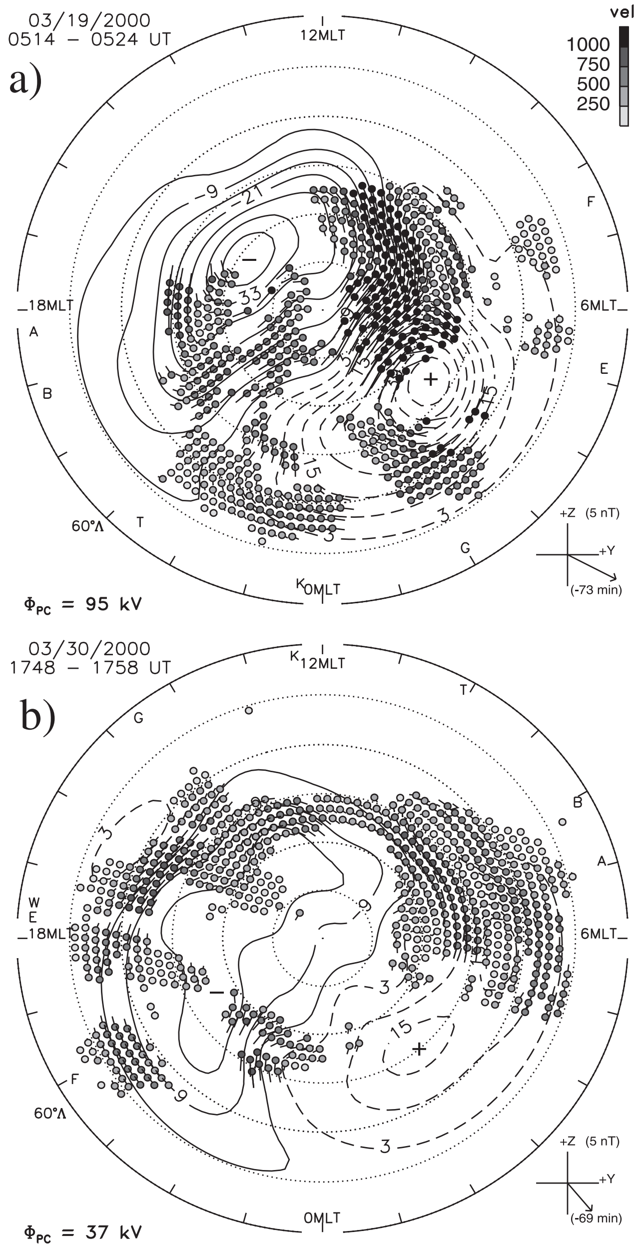

Figure 7. Two periods with E_{KL} = ~15 kV R_E^{-1} showing a relatively (a) high (95 kV) value of Φ_{PC} and (b) low (37 kV) value of Φ_{PC}, which correspond to the points marked 0 and 1 in Figure 4b, respectively.

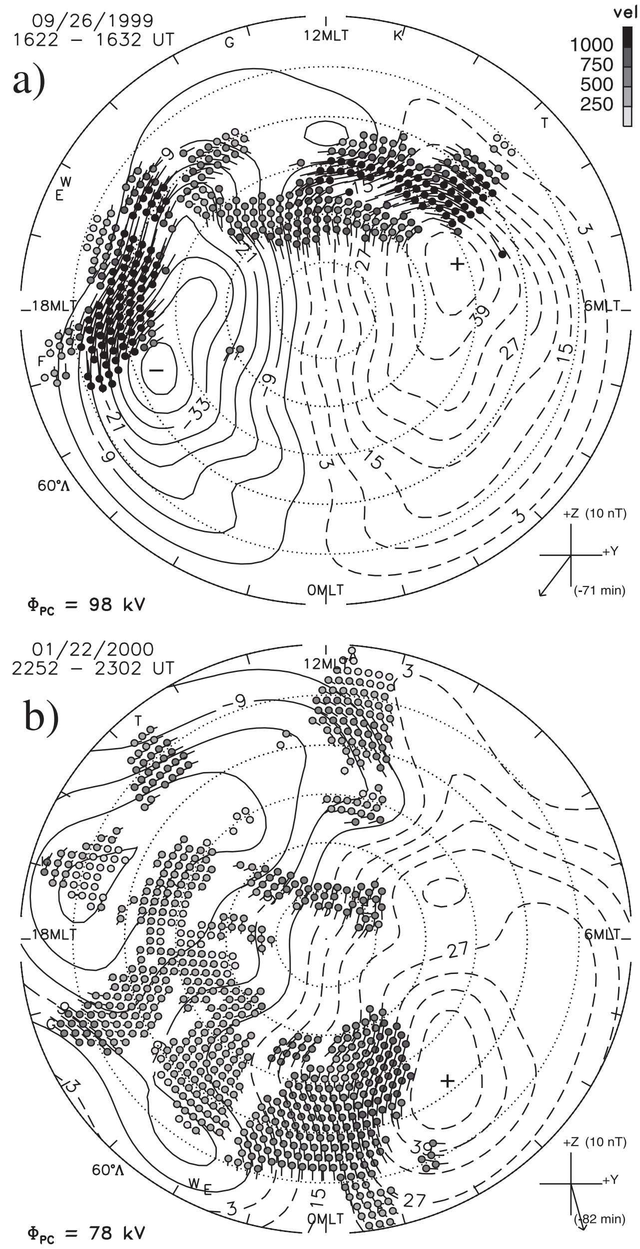

Figure 8. Two periods with E_{KL} = ~35 kV R_E^{-1} showing a relatively (a) high (98 kV) value of Φ_{PC} and (b) low (78 kV) value of Φ_{PC}, which correspond to the points marked 2 and 3 in Figure 4b, respectively.

from the Region 1 current system in terms of the solar wind parameters. Their model saturates for large values of E_{KL}; however, a further study is necessary to confirm whether the model matches the data presented in our study.

4. Summary

[46] We have carefully selected a set of 10-min-averaged periods from February 1998 through December 2000 to study the relationship between the solar wind and IMF conditions and Φ_{PC}. The periods were chosen such that (1) the solar wind and IMF conditions at the ACE spacecraft were quasi-stable for $\geq$40 min and (2) the coverage of

SuperDARN backscatter was adequate to determine Φ_{PC}. To satisfy the stability criteria it was decided that the effective interplanetary electric field E_{KL} could not vary by more than 7% for the $\geq$40-min period, making the calculation of the transit time from ACE to the ionosphere less critical. Suitable ionospheric coverage is defined as those times when >200 SuperDARN data points exist in the dayside sector (0600–1800 MLT) or >400 data points exist anywhere in the high-latitude region. A total of 9464 10-min-averaged periods were found to satisfy the first criteria, and a subset of 2721 10-min periods satisfied both criteria. By dropping the first and last 10-min period of each event, 1638 high-confidence periods remain.

[47] The resulting solutions of Φ_{PC} obtained by applying the APL FIT technique to the set of 10-min-averaged periods show that for quasi-steady solar wind and IMF, Φ_{PC} (1) is nonlinear in E_{KL}, (2) saturates at high values of E_{KL}, and (3) is extremely variable for all values of E_{KL}. These results indicate that simple formulations involving the upstream solar wind and IMF conditions are inadequate to describe the instantaneous Φ_{PC} in anything but a statistical sense. A model that includes internal processes, such as that developed by *Hill et al.* [1976] and *Siscoe et al.* [2002], is necessary to describe the relationship between the solar wind parameters, Φ_{PC}, and possibly other geomagnetic parameters. Further study is necessary to confirm the fit of these models with the data in our study.

[48] **Acknowledgments.** This work was supported by NSF grant ATM-[9812078] and NASA grant NAG5-[8361]. Operation of the Northern Hemisphere SuperDARN radars is supported by the national funding agencies of the U.S., Canada, the U.K., and France. We gratefully acknowledge the ACE/MAG instrument team, the ACE/SWEPAM instrument team, and the ACE Science Center for providing the ACE level 2 data. S. G. Shepherd gratefully acknowledges J. P. G. Shepherd for his assistance in estimating uncertainties in the ACE data.

[49] Janet G. Luhmann thanks Mark Lester and another referee for their assistance in evaluating this paper.

References

Baker, K. B., and S. Wing, A new coordinate system for conjugate studies at high latitudes, *J. Geophys. Res.*, *94*, 9139, 1989.

Boyle, C. B., P. H. Reiff, and M. R. Hairston, Empirical polar cap potentials, *J. Geophys. Res.*, *102*, 111, 1997.

Burke, W. J., D. R. Weimer, and N. C. Maynard, Geoeffective interplanetary scale sizes derived from regression analysis of polar cap potentials, *J. Geophys. Res.*, *104*, 9989, 1999.

Collier, M. R., J. A. Slavin, R. P. Lepping, A. Szabo, and K. Ogilvie, Time accuracy for the simple planar propagation of magnetic field structures in the solar wind, *Geophys. Res. Lett.*, *25*, 2509, 1998.

Coroniti, F. V., and C. F. Kennel, Can the ionosphere regulate magnetospheric convection?, *J. Geophys. Res.*, *78*, 2837, 1973.

Crooker, N. U., Dayside merging and cusp geometry, *J. Geophys. Res.*, *84*, 951, 1979.

Doyle, M. A., and W. J. Burke, S3-2 measurements of the polar cap potential, *J. Geophys. Res.*, *88*, 9125, 1983.

Fedder, J. A., and J. G. Lyon, The solar wind–magnetosphere–ionosphere current-voltage relationship, *Geophys. Res. Lett.*, *14*, 880, 1987.

Greenwald, R. A., K. B. Baker, J. M. Ruohoniemi, J. R. Dudeney, M. Pinnock, N. Mattin, J. M. Leonard, and R. P. Lepping, Simultaneous observations of dynamic variations in high-latitude dayside convection due to changes in IMF B_y, *J. Geophys. Res.*, *95*, 8057, 1990.

Greenwald, R. A., W. A. Bristow, G. J. Sofko, C. Senior, J.-C. Cerisier, and A. Szabo, Super Dual Auroral Radar Network radar imaging of dayside high-latitude convection under northward interplanetary magnetic field: Toward resolving the distorted two-cell versus multicell controversy, *J. Geophys. Res.*, *100*, 19,661, 1995.

Heelis, R. A., The effects of interplanetary magnetic field orientation on dayside high latitude ionospheric convection, *J. Geophys. Res.*, *89*, 2873, 1984.

Heppner, J. P., Polar-cap electric field distributions related to the interplanetary magnetic field direction, *J. Geophys. Res.*, *77*, 4877, 1972.

Heppner, J. P., and N. C. Maynard, Empirical high-latitude electric field models, *J. Geophys. Res.*, *92*, 4467, 1987.

Hill, T. W., A. J. Dessler, and R. A. Wolf, Mercury and Mars: The role of ionospheric conductivity in the acceleration of magnetospheric particles, *Geophys. Res. Lett.*, *3*, 429, 1976.

Kan, J. R., and L. C. Lee, Energy coupling function and solar wind–magnetosphere dynamo, *Geophys. Res. Lett.*, *6*, 577, 1979.

Khan, H., and S. W. H. Cowley, Observations of the response time of high-latitude ionospheric convection to variations in the interplanetary magnetic field using EISCAT and IMP-8 data, *Ann. Geophys.*, *17*, 1306, 1999.

Lester, M., O. de la Beaujardière, J. C. Foster, M. P. Freeman, H. Lühr, J. M. Ruohoniemi, and W. Swider, The response of the large scale ionospheric convection pattern to changes in the IMF and substorms: Results from the SUNDIAL 1987 campaign, *Ann. Geophys.*, *11*, 556, 1993.

Lyons, L. R., The geospace modeling program grand challenge, *J. Geophys. Res.*, *103*, 14,781, 1998.

Maynard, N. C., W. J. Burke, P. E. Sandholt, J. Moen, D. M. Ober, M. Lester, D. R. Weimer, and A. Egeland, Observations of simultaneous effects of merging in both hemispheres, *J. Geophys. Res.*, *106*, 24,551, 2001.

Papitashvili, V. O., B. A. Belov, D. S. Faermark, Y. I. Feldstein, S. A. Golyshev, L. I. Gromova, and A. E. Levitin, Electric potential patterns in the northern and southern polar regions parameterized by the interplanetary magnetic field, *J. Geophys. Res.*, *99*, 13,251, 1994.

Papitashvili, V. O., F. J. Rich, M. A. Heinemann, and M. R. Hairston, Parameterization of the Defense Meteorological Satellite Program ionospheric electrostatic potentials by the interplanetary magnetic field strength and direction, *J. Geophys. Res.*, *104*, 177, 1999.

Peredo, M., J. A. Slavin, E. Mazur, and S. A. Curtis, Three-dimensional position and shape of the bow shock and their variation with Alfvènic, sonic and magnetosonic Mach numbers and interplanetary magnetic field orientation, *J. Geophys. Res.*, *100*, 7907, 1995.

Prikryl, P., R. A. Greenwald, G. J. Sofko, J. P. Villain, C. W. S. Ziesolleck, and E. Friis-Christensen, Solar-wind-driven pulsed magnetic reconnection at the dayside magnetopause, Pc5 compressional oscillations, and field line resonances, *J. Geophys. Res.*, *103*, 17,307, 1998.

Reiff, P. H., and J. L. Burch, IMF B_y-dependent plasma flow and Birkeland currents in the dayside magnetosphere: A global model for northward and southward IMF, *J. Geophys. Res.*, *90*, 1595, 1985.

Reiff, P. H., and J. G. Luhmann, Solar wind control of the polar-cap potential, in *Solar Wind–Magnetosphere Coupling*, edited by Y. Kamide and J. A. Slavin, p. 453, Terra Sci., Tokoyo, 1986.

Reiff, P. H., R. W. Spiro, and T. W. Hill, Dependence of polar cap potential drop on interplanetary parameters, *J. Geophys. Res.*, *86*, 7639, 1981.

Rich, F. J., and M. Hairston, Large-scale convection patterns observed by DMSP, *J. Geophys. Res.*, *99*, 3827, 1994.

Richmond, A. D., and Y. Kamide, Mapping electrodynamic features of the high-latitude ionosphere from localized observations: Technique, *J. Geophys. Res.*, *93*, 5741, 1988.

Ridley, A. J., Estimations of the uncertainty in timing the relationship between magnetospheric and solar wind processes, *J. Atmos. Sol. Terr. Phys.*, *62*, 757, 2000.

Ridley, A. J., G. Lu, C. R. Clauer, and V. O. Papitashvili, A statistical study of the ionospheric convection response to changing interplanetary magnetic field conditions using the assimilative mapping of ionospheric electrodynamics technique, *J. Geophys. Res.*, *103*, 4023, 1998.

Ruohoniemi, J. M., and K. B. Baker, Large-scale imaging of high-latitude convection with Super Dual Auroral Radar Network HF radar observations, *J. Geophys. Res.*, *103*, 20,797, 1998.

Ruohoniemi, J. M., and R. A. Greenwald, Statistical patterns of high-latitude convection obtained from Goose Bay HF radar observations, *J. Geophys. Res.*, *101*, 21,743, 1996.

Ruohoniemi, J. M., S. G. Shepherd, and R. A. Greenwald, The response of the high-latitude ionosphere to IMF variations, *J. Atmos. Sol. Terr. Phys.*, *64*, 159, 2002.

Shepherd, S. G., and J. M. Ruohoniemi, Electrostatic potential patterns in the high latitude ionosphere constrained by SuperDARN measurements, *J. Geophys. Res.*, *105*, 23,005, 2000.

Shepherd, S. G., J. M. Ruohoniemi, R. A. Greenwald, and K. B. Baker, Improvements in the determination of Φ_{PC} from SuperDARN measurements, *Eos Trans. AGU*, *81*(48), Fall Meet. Suppl., p. F934, abstract SA62A-05, 2000.

Sibeck, D. G., R. E. Lopez, and E. C. Roelof, Solar wind control of the magnetopause shape, location, and motion, *J. Geophys. Res.*, *96*, 5489, 1991.

Sibeck, D. G., R. E. Lopez, and E. C. Roelof, Reply to comment by M. W. Dunlop, M. P. Freeman, and C. J. Farrugia on "Solar wind control of the magnetopause shape, location, and motion'', *J. Geophys. Res.*, *97*, 10,879, 1992.

Siscoe, G. L., and T. S. Huang, Polar cap inflation and deflation, *J. Geophys. Res.*, *90*, 543, 1985.

Siscoe, G. L., G. M. Erickson, B. U. Ö. Sonnerup, N. C. Maynard, J. A. Schoendorf, K. D. Siebert, D. R. Weimer, W. W. White, and G. R. Wilson, Hill model of transpolar potential saturation: Comparisons with MHD simulations, *J. Geophys. Res.*, 10.1029/2001JA000109, in press, 2002.

Slinker, S. P., J. A. Fedder, J. M. Ruohoniemi, and J. G. Lyon, Global MHD simulation of the magnetosphere for November 24, 1996, *J. Geophys. Res.*, *106*, 361, 2001.

Sojka, J. J., R. W. Schunk, and W. F. Denig, Ionospheric response to the sustained high geomagnetic activity during the March '89 great storm, *J. Geophys. Res.*, *99*, 21,341, 1994.

Sonnerup, B. U. Ö., Magnetopause reconnection rate, *J. Geophys. Res.*, *79*, 1546, 1974.

Spreiter, J. R., and S. S. Stahara, Gasdynamic and magnetohydrodynamic modeling of the magnetosheath: A tutorial, *Adv. Space Res.*, *14*(7), 5, 1994.

Weimer, D. R., Models of high-latitude electric potentials derived with a least error fit of spherical harmonic functions, *J. Geophys. Res.*, *100*, 19,595, 1995.

Weimer, D. R., A flexible, IMF dependent model of high-latitude electric potentials having ''space weather'' applications, *Geophys. Res. Lett.*, *23*, 2549, 1996.

Weimer, D. R., An improved model of ionospheric electric potentials including perturbations and application to the Geospace Environment Modeling November 24, 1996, event, *J. Geophys. Res.*, *106*, 407, 2001.

R. A. Greenwald and J. M. Ruohoniemi, Applied Physics Laboratory, Johns Hopkins University, 11100 Johns Hopkins Road, Laurel, MD 20723, USA. (raymond.greenwald@jhuapl.edu; mike.ruohoniemi@jhuapl.edu)

S. G. Shepherd, Thayer School of Engineering, Dartmouth College, 8000 Cummings Hall, Hanover, NH 03755-8000, USA. (simon.shepherd@dartmouth.edu)